Designed Functional Systems from Peapod-like Co@Carbon to Co_3O_4@Carbon Nanocomposites

Yu Wang,[†,*] Hui Juan Zhang,[‡] Li Lu,[§] Ludger Paul Stubbs,[†] Chee Cheong Wong,[‡] and Jianyi Lin[†,*]

[†]Institute of Chemical and Engineering Sciences (ICES), 1, Pesek Road, Jurong Island, Singapore, 627833, [‡]School of Materials Science and Engineering, Nanyang Technological University (NTU), 50 Nanyang Avenue, Singapore 639798, and [§]Department of Mechanical Engineering, National University of Singapore (NUS), Singapore 117576

ABSTRACT Novel peapod-like Co@carbon and Co_3O_4@carbon composite nanostructures have been successfully fabricated for the first time based on rational design and elaborate analyses. The nanostructures exhibit the unique feature of Co or Co_3O_4 nanoparticles (20 nm) encapsulated inside and well-graphitized carbon layers coating outside. The peapod-like Co@carbon and Co_3O_4@carbon nanostructures exhibit intriguing morphologies, architectures, and chemical compositions. What is more important, the unique morphologies, architectures, and chemical compositions will lead to perfect performances in many applications. In this paper, a good example of Li-ion battery testing is given to demonstrate the superior stability and rate capability of the Co_3O_4@carbon. The peapod-like nanostructure of Co_3O_4@carbon demonstrates very high specific capacity (around 1000 mAh/g at the charge/discharge rate of 1C) and wonderful cyclability (at least 80% retention is available when cycled back from very high charge/discharge rate of 10C) during the galvanostatic cycling, indicating it as the promising candidate for Li-ion batteries' anodes. Additionally, the excellent electrochemical performance is significantly associated with the unique architecture in the samples, which verifies the feasibility of rational design of hierarchical materials for the actual applications. Meanwhile, the Co@carbon and Co_3O_4@carbon nanostructures demonstrate the regular and uniform distribution of magnetic nanoparticles in well-graphitized carbon fiber, which is a great achievement in the field of monodispersing and isolating magnetic nanoparticles. The prepared samples can also be potentially applied in other fields, such as gene delivery, catalysis, and magnetism.

KEYWORDS: cobalt · carbon · lithium · hierarchical · energy storage

The controllable and selective synthesis of nanostructured materials is gradually becoming more important due to their functionalities and applications in plenty of fields, especially in biomedical, energy related, and electronic areas.[1−3] The combination of active materials and ancillary materials to form functional systems is highly expected to be a valid approach to achieve the designed synthesis. For the active materials, transition-metal oxides are regarded as the promising candidates since they exhibit unique and irreplaceable properties in optics, magnetism, catalysis, and electricity.[4,5] Certainly their potential functions in the energy field such as in electrochemical energy storage[6] may not be neglected either. Solid-state rechargeable batteries, in particular, Li-based batteries, have long been considered as an intriguing medium to store electrical power with respect to a wide variety of portable applications.[7−9] Li-ion batteries (LIBs) have the needed characteristics of high power/energy densities, long cycle life, environmental friendliness and safety and because of these have attracted the widespread interest of the world. However, there still have been some great challenges in the design of LIBs since the related technology was realized.[10,11] One of the emphases is how to enhance the specific capacity and improve the capacity retention over many charge−discharge cycles in the electrochemical performance of LIBs, which usually suffer from pulverization of the electrode material and Li-alloying agglomeration and amorphization during cycling.[12,13] Any changes evolved in the electrode materials will most probably result in deterioration for the system's electronic conductivity, ionic transport, and electrolyte diffusion. Thus we have to design one effective architecture to maintain the integrety of the electrode material and prevent its disintegration for the most part, in order to enhance the cyclability and rate capabilities of the batteries as actually required. For this aim, it is reasonably believed that nanotechnology is the golden key to solve the big problem in front of us. This belief arises from the fact that nanostructured materials prepared under precise control are desirable for the improvement in surface areas expansion, organization of electrode components, and electrolyte penetration.[14−16] Meanwhile, it is worth noting that nanosized particles are highly capable of catalyzing electrochemical reactions and electrolyte reversible degradation, which greatly contribute to the cycleable

*Address correspondence to wang_yu@ices.a-star.edu.sg.

Received for review March 2, 2010 and accepted July 22, 2010.

Published online July 28, 2010.
10.1021/nn1004183

capacities. However, the conventional nanotechnology is not expectedly qualified to fully demonstrate the advantages of nanomaterials over their counterparts in bulk. A good example given here is that as long as electrochemical cycling is imposed on pure nanostructured electrode materials their textural or structural integrity will be destroyed, and thus capacity retention is determined to be impaired accordingly. So the limited lifespans are frequently detected from those simplistic systems, regardless of their structures being represented with free-standing, randomly dispersed, or uniformly organized characters.[17−21] The ideal design of electrode materials at the nanoscale can be ascribed to synthesis of core−shell architectures consisting of mesoporours carbon shells located outside and active materials embedded inside.[21−27] In this case, the outer mesoporous carbon shells not only construct the conducting pathway for the system's electron transfer but also prevent the inner active materials from collapsing so as to sustain as much lithiation as the system is able to support.

As for the elementary active substance of metallic tin, the mechanism to store lithium is based on Li-alloying process, where formation of $Li_{4.4}Sn$ alloy is the intrinsic driving source for electrochemical activity in a negative electrode.[17,18,21−23,27] The same mechanism applies for some other elementary active materials as well, such as Si,[25,26,28] Ge,[29,30] and Au.[31] However, a big problem simultaneously arises that, accompanying the Li^+ insertion into these elementary substances and extraction from the formed alloys, tremendous changes in volume may result in the destruction of the initial structure and these changes have to be compensated for by the surrounding void spaces subsequently.[21−23,25,26,28−30] To transcend the encountered barrier, we need to consider designing excess void spaces in carbon hollow structures; however, that will inevitably decrease the volumetric deliverable power/energy densities with respect to the total systems.

Transition-metal oxides, for example, Co_3O_4, Fe_3O_4, MnO_2, follow another distinct reaction route to achieve the lithium storage, where the conventional reduction/oxidation processes take place through the chemical equation

$$M_xO_y + 2_yLi \rightleftharpoons xM + yLi_2O \quad (1)$$

M represents the transition metal. The negative effect from the volume expansion may be avoided for the most part using transition-metal oxides as anodic materials for LIBs. However, to date, few reports have been involved in the fabrication of hybrid core−shell structures from other active materials except for SnO_2 or Sn. In our consideration, Co_3O_4 demonstrates a high theoretical capacity of 890 mAh/g, more than twice that of the currently commercial negative electrode material, graphite (372 mAh/g). Additionally, as a catalytically active element, the metallic Co nanoparticles generated from the reduction process while discharging are favorable for the reversible formation of polymeric layer originating from the electrolyte decomposition.[31,34] Hence, an extra contribution to the enhanced lithium storage will be considerably provided through this way. Furthermore, the solid-electrolyte interface (SEI) developed from the electrochemical reactions will also absorb excess Li ions for the improved Li storage efficiency.[31,34] Combined with the above considerations, it turns out that design and synthesis of core−shell architecture from carbon and Co_3O_4 will be an attractive technology of choice for the growing electrochemical energy storage demands from portable electronics and mobile telecommunication devices. Of course, the hierarchical architecture can also be applied in biomedical areas such as gene delivery.

RESULTS AND DISCUSSION

Herein we report a rational and facile method to generate peapod-like Co_3O_4@carbon hierarchical architecture for the first time with the ability to at least deliver 91% (1050 mAh/g) of the total capacity (1144 mAh/g, the onset value of the stable power delivery from the second cycle) after 50 cycles at charge/discharge rate of 1C (1C is defined as one lithium per formula in an hour and for Co_3O_4@Carbon, 1C is equivalent to 100 mA/g in our experiment). During the experiments of rate capability and cyclability, approximately 80% retention of the discharge capacity was recovered from higher charge−discharge rates (2.5C, 5C, and 10C for 10 cycles, respectively) when cycled back to 1C. The synthesis of such a unique hybrid structure thoroughly adopted a templated strategy based on the previous formation of cobalt carbonate hydroxide ($Co(CO_3)_{0.5}(OH)0.11H_2O$) nanobelts. Subsequently under the aid of the hydrogen-bonding action among the many hydroxyl groups spreading across the glucose molecules and the surfaces of $Co(CO_3)_{0.5}(OH)0.11H_2O$ nanobelts, polymerized glucose layers had successfully been coated onto the nanobelts' surfaces. Then experiencing a thermal treatment in inert atmosphere and additional calcinations at 250 °C in air, the nanobelts with the polymeric layers coating were finally converted into the targeted products of core−shell Co_3O_4@carbon nanostructure.

The overall synthetic procedure is described in Scheme 1 based on the previous results.[14] Because hydroxyl groups are one of the constituents in $Co(CO_3)_{0.5}(OH)0.11H_2O$, plenty of hydrates also offer the possibility of hydrogen bonding between glucose and $Co(CO_3)_{0.5}(OH)0.11H_2O$ molecules, and it is a feasible idea to coat the polymeric layer on $Co(CO_3)_{0.5}(OH)0.11H_2O$ nanobelts through the hydrothermal method (step 1). After necessary washing and drying, the samples are calcined in an inert atmosphere

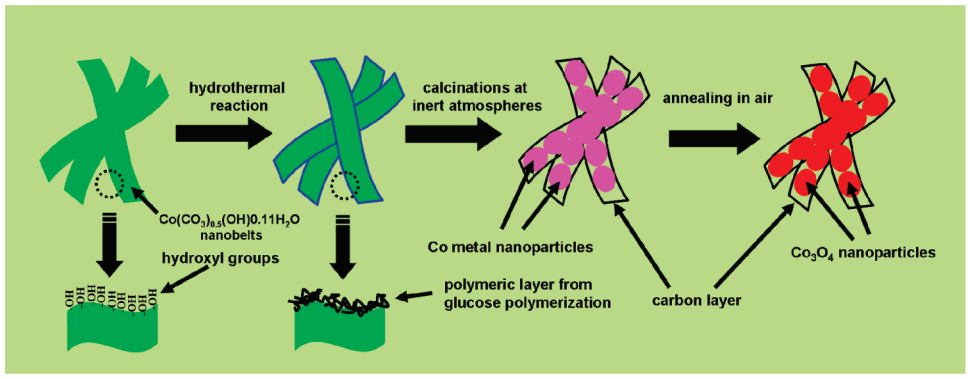

Scheme 1. Schematics to illustrate the synthetic procedure of the peapod-like Co_3O_4@carbon nanocomposite. Based on the formation of the precursor $Co(CO_3)_{0.5}(OH)0.11H_2O$ nanobelts, polymeric layers from glucose polymerization are successfully coated on the surfaces of the nanobelts through the hydrogen bonding between $Co(CO_3)_{0.5}(OH)0.11H_2O$ and glucose molecules under hydrothermal conditions (step 1, the locally enlarged regions describe the hydroxyl groups on the surfaces of the $Co(CO_3)_{0.5}(OH)0.11H_2O$ nanobelts and the polymerized layers coated on nanobelts' surfaces from glucose polymerization). The coating polymeric layers will be carbonized to graphitized carbon layers after calcination in inner atmosphere at high temperature (see Experimental Section) to generate peapod-like Co@carbon nanocomposites (step 2). Then the Co nanoparticles encapsulated in the carbon fibers will be converted to Co_3O_4 nanoparticles, through which to form the ultimate peapod-like Co_3O_4@carbon nanocomposite when annealed in air (step 3).

of Ar at 700 °C for 200 min to generate the transitional product of metallic Co nanoparticles encapsulated in carbon fibers (step 2). Subsequently, the intermediate product is annealed in air at 250 °C for 200 min to yield the finally outstanding samples (step 3).

Scanning electron microscopy (SEM) and scanning transmission electron microscopy (STEM) were employed to investigate the as-collected samples as shown in Figure 1. Figure 1 panels a and b are the typical SEM images. From Figure 1a it is revealed that the samples could be prepared in large scale in our experiments. The corresponding magnified SEM image shown in Figure 1b indicates that the samples exhibit uniform belt-shaped morphology with lengths up to several micrometers and diameters down to 50 nm. Interestingly, along the nanobelts' axial direction, some nanoparticles are always dotted and extended (Figure 1b). To obtain the structural details about the samples, STEM was used to collect more information as displayed in Figure 1c,d. From both images, in particular, Figure 1d, it is detected that the nanoparticles with around 30 nm in diameter are monodispersed along the same direction with periodic intervals. A transparent thin layer under e-beam irradiation with an accelerating voltage of 30 kV is found to encapsulate and confine the nanoparticles making the samples just like peapods.

By means of X-ray diffraction (XRD) characterization we traced the overall transitional process as indicated

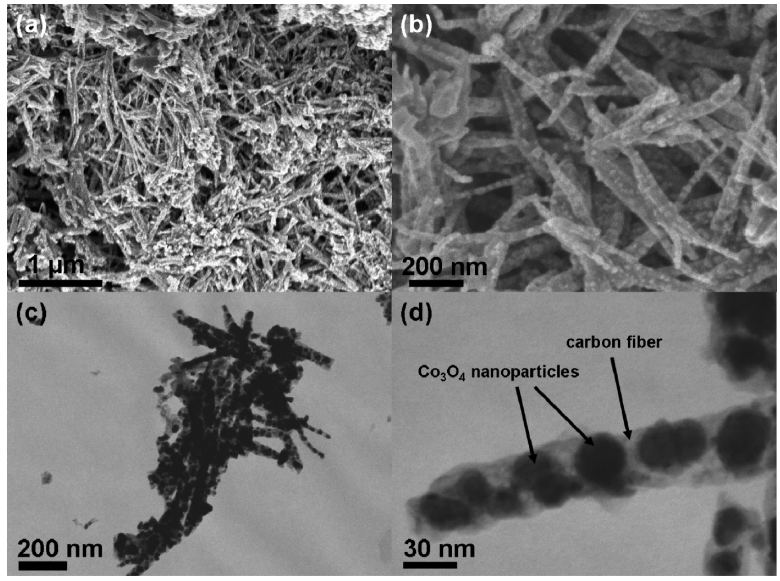

Figure 1. (a,b) Typical scanning electron microscopy (SEM) images. From panel a, large scale production of the peapod-like Co_3O_4@carbon nanocomposite samples can be clearly detected. From panel b, some peapod-like structures with some nanoparticles dotted in line can be observed. The scanning transmission electron microscopy (STEM) images (c,d) show the confirmative information about the peapod-like structures for our samples. Especially in image d can we see that some nanoparticles with 20−30 nm in diameter are monodispersed in tubular fibers with regular intervals.

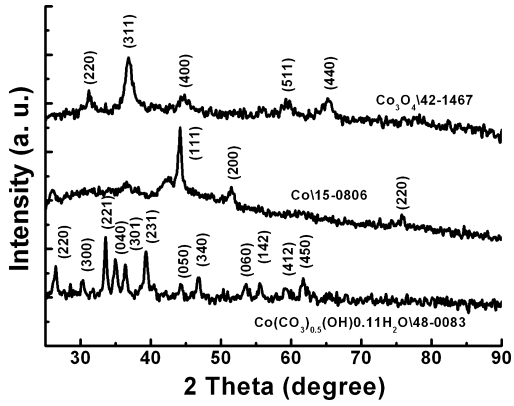

Figure 2. X-ray diffraction (XRD) patterns are collected to trace the conversion processes from $Co(CO_3)_{0.5}(OH)0.11H_2O$ to Co and finally to Co_3O_4 in our samples. From bottom to top, the XRD patterns are determined to be $Co(CO_3)_{0.5}(OH)0.11H_2O$, metallic Co, and Co_3O_4 in sequence after elaborate analyses.

in Figure 2. From bottom to top, three distinct XRD patterns correspond to $Co(CO_3)_{0.5}(OH)0.11H_2O$ (JCPDS No. 48-0084), Co (JCPDS No. 15-0806), and Co_3O_4 (JCPDS No. 42-1467) in sequence, implying the total conversion from the precursors to intermediate products, and finally to the targeted samples; meanwhile, transmission electron microscopy (TEM) and high-resolution TEM (HRTEM) were adopted to achieve further evidence about the transitional process. In Figure 3, the left column (panels a, c, and e) exhibits the representative TEM images of $Co(CO_3)_{0.5}(OH)0.11H_2O$ nanobelts (top), peapod-like Co@carbon core−shell fibers (middle), and peapod-like Co_3O_4@carbon core−shell fibers (bottom). On the basis of these images, we can find that, derived from our experimental conditions, samples will be fabricated uniformly and be remained unchanged in morphologies, revealing that the originally designed synthetic strategy successfully leads to the destined samples. HRTEM technique provided more detailed information in the structure of the samples as described and indexed in the right column of Figure 3, where locally enlarged HRTEM images can be detected from the rectangular regions marked in the corresponding low-magnification TEM images. The significant difference in the three crystal structures clearly verifies that the samples are ascribed to three differentiated materials. Additionally, the presence of graphitic layers as determined in Figure 3d,f and the low magnification TEM images of Figure 3c,e, together with the absence of carbon layer in the precursors as certified in Figure 3b tells us the designed hierarchical structure definitely resulted from the smooth coating of glucose on $Co(CO_3)_{0.5}(OH)0.11H_2O$ nanobelts and the following thermal treatments. To the best of our knowledge, until now there have been few reports involving the successful coating of a carbon layer on Co_3O_4 nanostructures, especially to produce monodisperse samples. So far, the most studied material in the previous reports involving the carbon coating is SnO_2. Owing to the many hydroxyl groups evenly extending across the surface of the material, SnO_2 is highly capable of absorbing other molecules abounding in the hydroxyl groups, inclusive of glucose molecules, to ultimately yield a hybrid structure with the polymerized layer coated through the hydrothermal method. Of course, a polymeric layer from glucose polymerization may be coated onto other materials. However, such a situation is scarcely reported. So in our case, we have detected another material with the ability to be coated directly with polymerized glucose other than SnO_2.[21,23] By means of Raman spectrum, the simultaneous presence of graphitized carbon and well-crystallized Co_3O_4 in our final samples is completely determined (Supporting Information). Additionally, in our case, we have successfully synthesized isolated and monodisperse magnetic nanoparticles of Co and Co_3O_4 encapsulated in well-graphitized carbon fibers, which will be of great interest in studies of magnetism, gene imaging, gene delivery, or catalysis.

Compared to the Li alloying process in other active materials for LIBs, such as Si, Ge, Sn, and Au, Co_3O_4 exhibits the Li-storage activity for LIBs through reduction/oxidation reactions, where Co_3O_4 is reduced to CoO first, then to elemental Co while discharging, and afterward oxidized back or partially oxidized back to its initial state while charging; meanwhile, Li is joining in the cycling process shuttling between the elemental state and the oxidative state of Li_2O. The theoretical capacity for Co_3O_4 is estimated to be 890 mAh/g according to[35]

$$Co_3O_4 + 8Li \rightleftharpoons 3Co + 4Li_2O \qquad (2)$$

As shown in Figure 4a, cyclic voltammetry (CV) was applied to investigate the electrochemical details when the cell was set to be scanned at 0.5 mV/s within the voltage window of 0.01−3.00 V. The cathodic scan for the first cycle reveals two peaks at voltage positions of 1.14 and 0.87 V accompanied with the reduction processes of Co^{3+} to Co^{2+} and Co^{2+} to Co, respectively (Figure 4a, red curve). During the subsequent cycling, the CV profiles tend to be stable. To have a comparison between the first cycle and following ones, the CV curve of the tenth cycle was selected to highlight the difference (Figure 4a, black curve), wherein a little shift to the low potential at voltage positions of 1.10 and 0.85 V for the reduction peaks of the tenth cycle is clearly detected. The shift implies that the actual Li-ion battery assembled from our hybrid Co_3O_4/carbon peapod-like samples as anode and other layered materials, for example, $LiCoO_2$ as cathode, would have a little higher working potential with the cycling going on.[36] Nevertheless, the current densities, whatever are the current densities during cathodic scan or anodic scan, are becoming a little weaker than that of the initial state, indicating some irreversible electrochemical processes oc-

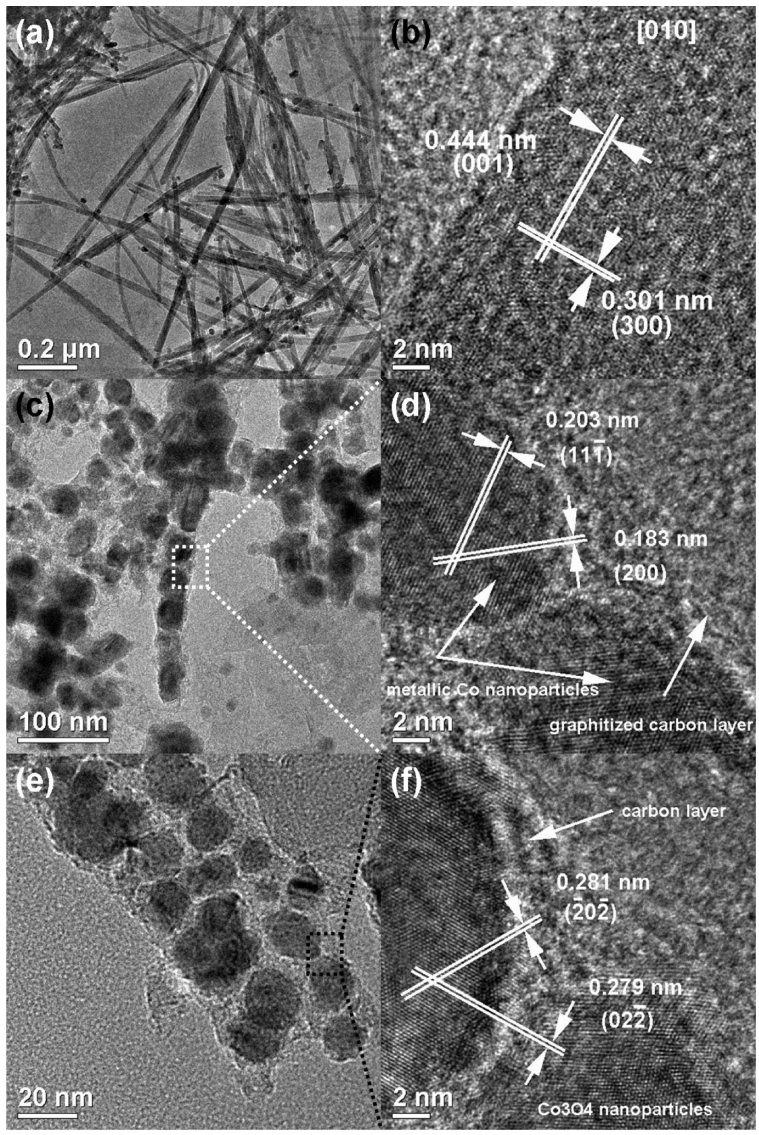

Figure 3. (a) Low-magnification transmission electron microscopy (TEM) image to confirm the uniformity and regularity of our precursors. The corresponding high-resolution TEM (HRTEM) image (b) indicates that the $Co(CO_3)_{0.5}(OH)0.11H_2O$ nanobelts exhibit well-crystallized features. (c) TEM and (d) HRTEM images for the intermediate products of peapod-like Co@carbon nanocomposites which show that the encapsulated well-crystallized Co nanoparticles (d) are coated with carbon layers (c) to form the 1-D hierarchical structures. The ultimately synthesized peapod-like Co_3O_4@carbon nanocomposites exhibit well-crystallized feature as well (f) and meanwhile maintain the carbon layers unchanged during the annealing in air (e).

curred in the cell. The conclusion was also certified in the galvanostatic cycling, as described in Figure 4b. Still from Figure 4a, the upper cutoff voltage is estimated to be 1.393 V, lower than that of the conventional Co_3O_4 nanostructures,[37] matching well with the galvanostatic cycling profiles in Figure 4b. Galvanostatic cycling can provide straightforward evidence about electrochemical properties in reversibility and cyclability so that it was adopted in our experiments as indicated in Figure 4b. From Figure 4b, we can detect that from the second cycle onward until the fiftieth cycle, the peapod-like Co_3O_4@carbon samples exhibit excellent performance in the high specific capacities at a charge/discharge rate of 1C, symbolized with characteristics of supersteady power supply of 1050 mAh/g. As a comparison, Co_3O_4 nanoparticles with around 22 nm in diameter (Supporting Information) were tested in galvanostatic cycling when cycled at the conditions kept constant (Figure 4c). From Figure 4c, the cyclable ability of Co_3O_4 nanoparticles is observed to be significantly hampered because the nanoparticles inevitably were damaged after a long time cycling, resulting in aggregation and pulverization (Figure 4c, the circled line). The specific capacities of these nanoparticles fade rapidly to below 372 mAh/g, the theoretical capacity for graphite, within 20 cycles. After 50 cycles, their discharge capacities almost decay to 0 mAh/g, justifying the poor electrochemical performance. To further attest to the perfect cyclability and rate capability of our samples, the charge/discharge rates were programmably modified to increase

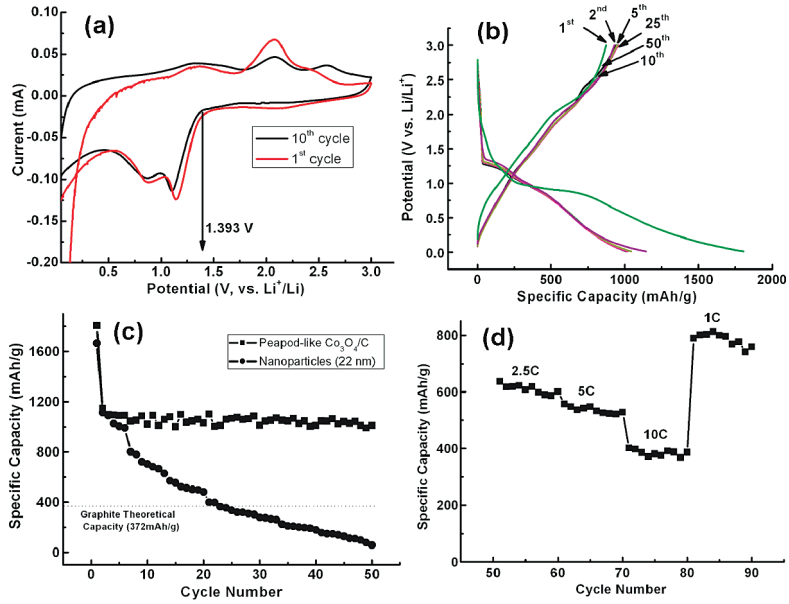

Figure 4. (a) Cyclic voltammetry (CV) profiles for the peapod-like Co_3O_4@carbon samples to reveal the samples' reduction/oxidation features and upper cutoff voltage of 1.393 V. (b) The curves associated with potential *versus* specific capacity. We can see that the power supplies from the peapod-like Co_3O_4@carbon nanocomposites are stabilized at discharge capacities of around 1000 mAh/g and meanwhile, the upper cutoff voltage is confirmed to be 1.393 V as verified in panel a. (c) Capacitive comparison between the peapod-like Co_3O_4@carbon nanocomposites (the squared line) and Co_3O_4 nanoparticles (22 nm, the dotted line) (Supporting Information) to highlight the excellent stability during long time cycling for the peapod-like structures. (d) Wonderful cyclability and good capacity retention of the samples when the charge/discharge rates increase gradually from 1C to 10C and decrease back to 1C is demonstrated.

from 1C for 50 cycles, stepwise to 2.5C for 10 cycles, 5C for 10 cycles, 10C for 10 cycles, then back to 1C for 10 cycles, and the corresponding discharge capacities were varied accordingly with the charge/discharge rates, changing from 1050, to 600, 530, and 380 mAh/g, finally reversibly back to 800 mAh/g (Figure 4d). Although the energy delivery loss of about 200 mAh/g occurs, the total retention of 80% based on the initial state is still highly expected from our samples. The excellent electrochemical properties for our samples embodied in the galvanostatic cycling demonstrate that the peapod-like hybrid Co_3O_4/carbon structure is a promising candidate for the anode material for LIBs and will be favorable for their actualized application in electrochemical energy storage. Furthermore, the outstanding electrochemical performance is tightly associated with the unique architecture in our samples, which has been elaborately designed and fabricated with the aim to scale up the advantages in the composite materials. These ultimate achievements have verified our prediction and will be of great importance for guiding the synthesis of designed functional materials or systems in the future.

In the previously reported results, the specific capacities higher than the theoretical value sometimes are mentioned.[31,34] The unique phenomenon is often attributed to the reversible decomposition of electrolyte with formation of solid-electrolyte-interphase (SEI) while cycling and extra absorption of Li ions in the mesoporous architectures or the simultaneously formed SEI.[31,34] For Co_3O_4 or other transition-metal oxides, frequently questioned issues arise because the oxidative process from metallic Li to Li_2O accompanied by discharging is believed to be a thermodynamically stable reaction; however, Li_2O is a well-known inactive material for LIBs and the inverse process with Li_2O reduction back to the involved metallic Li is not theoretically considered as a valid approach. So how can we design a functionized system or material to conquer the energy barriers and realize the reversible process that is crucial for the reversibility and cyclability of the LIBs? At the same time, the mechanical loss in active materials while cycling is inevitable, so how can we guarantee the electrical contact between active materials and electrode for electron transfer will be alleviated from the aggregation and pulverization of the active materials? To answer the first question, the reasonable explanation is given that, when the dimensions of the materials decrease down to nanoscale, the surface energies of the materials will be enhanced substantially so that the energy gaps will be filled up and the reversible reactions can proceed accordingly.[31,34] Normally, nanosized Co particles with several nanometers in diameter will be formed during discharging, and the formation of Co nanoparticles provides large amounts of active sites for the reversible catalytic reactions making the reversibility charateristic change from invalid to valid.[31,34] In our case, not only will the Co nanoparticles be generated, but also the overall size of Co_3O_4 particles encapsulated in carbon fibers will be regularly confined within 20−30 nm (Figure 1d), both of which considerably ensure our samples exhibit perfect reversibility and cyclability. All

the above presumptions have been verified in our following electrochemical investigations.

For the second question, we can give out a satisfactory answer as well. In our experiments, the novel core−shell nanocomposite structure supplies a dream model with the active material of Co_3O_4 nanoparticles encapsulated inside and protective as well as conductive graphitized carbon layers exposed outside. The graphitized parts in the coating carbon shell offer a fluent electrical pathway, and the amorphous parts provide a number of wonderful channels for electrolyte diffusion or Li-ion transport (Supporting Information). Additionally, the carbon shells prevent Co_3O_4 nanoparticles from aggregation and pulverization while cycling, and simultaneously the void spaces between the Co_3O_4 nanoparticles and the carbon shells originated from the reductive reaction following eq 3 when heated in inert atmosphere will accommodate the possible volume changes (Figures 1d, and 3e,f).

$$2Co(CO_3)_{0.5}(OH)0.11H_2O + C \rightarrow 2Co + 2CO_2 + 1.22H_2O \quad (3)$$

All the suggestions imply and support one predictable outcome that our samples will demonstrate wonderful electrochemical performance for LIBs.

CONCLUSION

We report a rational route to synthesize one kind of novel peapod-like composite Co@carbon and Co_3O_4@carbon structures, and realized the application in the anode of Li-ion batteries. The structures display the encapsulated architecture with Co or Co_3O_4 nanoparticles embedded inside and graphitic carbon layer coating outside. The preparation strategy totally depends on the hydrogen bonding between glucose molecules and $Co(CO_3)_{0.5}(OH)0.11H_2O$, and the polymerization process under hydrothermal conditions. Experiencing following calcinations in Ar and annealing in air in sequence, the intermediate products of Co@carbon are ultimately converted to the targeted samples of Co_3O_4@carbon. The samples exhibit both a well-crystallized feature for the Co or Co_3O_4 nanoparticles and a well-graphitized character for the carbon layer; meanwhile, some void spaces are formed during the thermal treatment in Ar accompanying the reduction of $Co(CO_3)_{0.5}(OH)0.11H_2O$ to Co and oxidation of carbon to CO_2 or CO. To the best of our knowledge, it is first time the fabrication of such a functionalized material made of Co/Co_3O_4 and carbon has been reported. As predicted, our samples exhibit perfect electrochemical properties when tested using cyclic voltammetry and galvanostatic cycling. The samples simultaneously demonstrate good rate capability and wonderful cyclability, which are attributed to the unique core−shell structure we obtained in our experiments, where carbon shells not only prevent Co_3O_4 nanoparticles from aggregation and pulverization, but also are desirable for the electron transfer. Moreover, the void spaces between Co_3O_4 nanoparticles and carbon shells will digest the possible volume changes while cycling. The small size of Co_3O_4 nanoparticles will increase the contact areas between electrolyte and active materials and improve the catalytic effects when recharged. All the above advantages over the conventional materials are subject to our rational design and enable our samples to be the highly qualified anode material for actual LIBs. Furthermore, the achieved Co/Co_3O_4 and carbon one-dimensional core−shell nanostructures can be employed in other important areas, such as gene delivery, magnetism, and catalysis (ethanol reforming and CO oxidation), and the related results will be presented soon.

MATERIALS AND METHODS

Materials. All chemicals or materials were used directly without any further purification prior to usage. Ethylene glycol (Fisher Chemical, 99.99%), ammonia hydroxide ($NH_3 \cdot H_2O$, 28−30 wt %, J.T.Baker), cobalt nitrate ($Co(NO_3)_2$, 99.9%, Aldrich), sodium carbonate (Na_2CO_3, 99.9%, Aldrich), titanium foil (0.127 mm (0.005 in.) thick, annealed, 99%, Alfa Aesar), D(+)-glucose (Cica-Reagent, Kanto Chemical), and metallic Li foil (99.9%, Aldrich).

Preparation of $Co(CO_3)_{0.5}(OH)0.11H_2O$ Nanobelts. In a typical synthesis, ethylene glycol (15−20 mL), concentrated $NH_3 \cdot H_2O$ (10−15 mL, 28 wt %), 1 M Na_2CO_3 aqueous solution (1−2 mL), and 1 M $Co(NO_3)_2$ aqueous solution (4−6 mL) were mixed step by step in intervals of 2 min under vigorous stirring. After that, another 20 min were introduced into the stirring period, and finally the mixture turned into a homogeneous solution with a deep dark color. Once the precursor was transferred into a Teflon-lined stainless steel autoclave with a volume of 45 mL, a thermal treatment was performed for the Teflon-liner in an electric oven at 170 °C for 16 h. After the autoclave was cooled down naturally to room temperature in a fumehood, samples deposited at the bottom were collected and washed by centrifugation for at least three cycles using deionized water (D.I. water) and one cycle using pure ethanol. The as-synthesized samples were then dried in a vacuum oven at 40 °C overnight to remove the absorbed water for the subsequent characterizations.

Preparation of Peapod-like Co_3O_4@Carbon Nanocomposite. $Co(CO_3)_{0.5}(OH)0.11H_2O$ nanobelts (100−300 mg) were ultrasonically mixed with glucose aqueous solution (5 mL, 1 M) together with additional D.I. water (20 mL) to form a homogeneous solution after 15 min. The above solution was introduced into a 45 mL Teflon-lined autoclave and sealed tightly. Then the liner was heated in an electric oven at 180 °C for 4 h. After that, the samples were washed by centrifugation for at least three cycles using deionized water (D.I. water) and one cycle using pure ethanol and then dried in air at 60 °C overnight to remove the residue water and ethanol. Afterward, the dried samples were loaded into the tube furnace and calcined in Ar atmosphere at 700 °C for 200 min with a ramp of 1 °C/min. Finally the samples were annealed at 250 °C for 200 min in air to oxidize the previously formed Co to Co_3O_4.

Characterization of the Samples. Scanning electron microscopy (SEM, FEI, 5 kV), field emission scanning electron microscope (FESEM, JEOL, JSM-7600F), transmission electron microscopy (TEM, Philips, Tecnai, F20, 200 kV), powder X-ray diffraction (XRD, Bruker D8 Advance X-ray diffractometer with Cu Kα radiation),

RENISHAW Invia Raman microscope (voltage (AC) 100−240 V, Power 150W, UK) were employed to characterize the obtained samples.

Electrochemical Characterization. A homogeneous mixture composed of active material and polyvinyl difluoride (PVDF) using 1-methyl-2-pyrrolidinone (NMP) as solvent in a weight ratio of 95:5 was prepared under strong magnetic stirring for at least 3 days. Then the mixture was extracted and spread on Ti foils. Before and after the samples were spread, the Ti foils were weighed in a high-precision analytical balance (Sartorius, max weight 5100 mg, $d = 0.001$ mg). The reading difference was the exact mass for the coated samples on Ti foils. The obtained pieces of Ti covered with samples were then used as working electrodes with 1 M LiPF6 in ethylene carbonate and diethyl carbonate (EC−DEC, v/v = 1:1) as electrolyte. Celgard 2400 was used as the separator film to isolate the two electrodes. Pure Li foil (99.9%, Aldrich) was used to serve as counter-electrode and reference electrode. The cell was assembled in an argon-filled glovebox where moisture and oxygen concentrations were strictly limited to below 1 ppm. The galvanostatic cycling was performed on Neware battery testing system, model 5 V1−5 mA, and cyclic voltammetry (CV) was collected using Autolab (model AUT71740) in a three-electrode cell. Li foil was used as counter-electrode (anode) and reference electrode.

Acknowledgment. We acknowledge financial support from Intelligent Energy Distribution Systems (IEDS) of Agency for Science, Technology, and Research (ASTAR) and Institute of Chemical and Engineering Sciences (ICES) in Singapore.

Supporting Information Available: Raman spectrum for the prepared nanocomposite and TEM images for Co_3O_4 nanoparticles. This material is available free of charge *via* the Internet at http://pubs.acs.org.

REFERENCES AND NOTES

1. Wang, Y.; Foo, C. Y.; Hoo, T. K.; Ng, M.; Lin, J. Y. Designed Smart System of the Sandwiched and Concentric Architecture of RuO_2/C/RuO_2 for High Performance in Electrochemical Energy Storage. *Chem.—Eur. J.* **2010**, *16*, 3598–3603.
2. Xie, X. W.; Li, Y.; Liu, Z. Q.; Haruta, M.; Shen, W. J. Low-Temperature Oxidation of CO Catalysed by Co_3O_4 Nanorods. *Nature* **2009**, *458*, 746–749.
3. Wang, Y.; Liao, Q.; Lei, H.; Zhang, X. P.; Ai, X. C.; Zhang, J. P.; Wu, K. Interfacial Reaction Growth: Morphology, Composition, and Structure Controls in Preparation of Crystalline $Zn_xAl_yO_z$ Nanonets. *Adv. Mater.* **2006**, *18*, 943–947.
4. Hu, L. H.; Peng, Q.; Li, Y. D. Selective Synthesis of Co_3O_4 Nanocrystal with Different Shape and Crystal Plane Effect on Catalytic Property for Methane Combustion. *J. Am. Chem. Soc.* **2008**, *130*, 16136–16137.
5. Liu, B.; Aydil, E. S. Growth of Oriented Single-Crystalline Rutile TiO_2 Nanorods on Transparent Conducting Substrates for Dye-Sensitized Solar Cells. *J. Am. Chem. Soc.* **2009**, *131*, 3985–3990.
6. Aurbach, D.; Lu, Z.; Schechter, A.; Gofer, Y.; Turgeman, H.; Cohen, Y.; Moshkovich, M.; Levi, E. Prototype Systems for Rechargeable Magnesium Batteries. *Nature* **2000**, *407*, 724–727.
7. Armand, M.; Tarascon, J. M. Building Better Batteries. *Nature* **2008**, *451*, 652–657.
8. Kang, K.; Meng, Y. S.; Bréger, J. L.; Grey, C. P.; Ceder, G. Electrodes with High Power and High Capacity for Rechargeable Lithium Batteries. *Science* **2006**, *311*, 977–980.
9. Tarascon, J. M.; Armand, M. Issues and Challenges Facing Rechargeable Lithium Batteries. *Nature* **2001**, *414*, 359–367.
10. Whittingham, M. S. Lithium Batteries and Cathode Materials. *Chem. Rev.* **2004**, *104*, 4271–4301.
11. Kang, B.; Ceder, G. Battery Materials for Ultrafast Charging and Discharging. *Nature* **2009**, *458*, 190–193.
12. Bruce, P. G.; Scrosati, B.; Tarascon, J. M. Nanomaterials for Rechargeable Lithium Batteries. *Angew. Chem., Int. Ed.* **2008**, *47*, 2930–2946.
13. Li, H.; Wang, Z. X.; Chen, L. Q.; Huang, X. J. Research on Advanced Materials for Li-ion Batteries. *Adv. Mater.* **2009**, *21*, 4593–4607.
14. Wang, Y.; Xia, H.; Lu, L.; Lin, J. Y. Excellent Performance in Lithium-Ion Battery Anodes: Rational Synthesis of $Co(CO_3)_{0.5}(OH)0.11H_2O$ Nanobelt Array and Its Conversion into Mesoporous and Single-Crystal Co_3O_4. *ACS Nano* **2010**, *3*, 1425–1432.
15. Hu, Y. S.; Guo, Y. G.; Dominko, R.; Gaberscek, M.; Jamnik, J.; Maier, J. Improved Electrode Performance of Porous $LiFePO_4$ Using RuO_2 as an Oxidic Nanoscale Interconnect. *Adv. Mater.* **2007**, *19*, 1963–1966.
16. Kim, M. G.; Cho, J. Reversible and High-Capacity Nanostructured Electrode Materials for Li-Ion Batteries. *Adv. Funct. Mater.* **2009**, *19*, 1497–1514.
17. Park, M. S.; Wang, G. X.; Kang, Y. M.; Wexler, D.; Dou, S. X.; Liu, H. K. Preparation and Electrochemical Properties of SnO_2 Nanowires for Application in Lithium-Ion Batteries. *Angew. Chem., Int. Ed.* **2007**, *46*, 750–753.
18. Liu, J. P.; Li, Y. Y.; Huang, X. T.; Ding, R. M.; Hu, Y. Y.; Jiang, J.; Liao, L. Direct Growth of SnO_2 Nanorod Array Electrodes for Lithium-Ion Batteries. *J. Mater. Chem.* **2009**, *19*, 1859–1864.
19. Taberna, P. L.; Mitra, S.; Poizot, P.; Simon, P.; Tarascon, J. M. High Rate Capabilities Fe_3O_4-Based Cu Nano-Architectured Electrodes for Lithium-Ion Battery Applications. *Nat. Mater.* **2006**, *5*, 567–573.
20. Li, Y. G.; Tan, B.; Wu, Y. Y. Mesoporous Co_3O_4 Nanowire Arrays for Lithium Ion Batteries with High Capacity and Rate Capability. *Nano Lett.* **2008**, *8*, 265–270.
21. Zhang, W. M.; Hu, J. S.; Guo, Y. G.; Zheng, S. F.; Zhong, L. S.; Song, W. G.; Wan, L. J. Tin-Nanoparticles Encapsulated in Elastic Hollow Carbon Spheres for High-Performance Anode Material in Lithium-Ion Batteries. *Adv. Mater.* **2008**, *20*, 1160–1165.
22. Lee, K. T.; Jung, Y. S.; Oh, S. M. Synthesis of Tin-Encapsulated Spherical Hollow Carbon for Anode Material in Lithium Secondary Batteries. *J. Am. Chem. Soc.* **2003**, *125*, 5652–5653.
23. Ye, J. F.; Zhang, H. J.; Yang, R.; Li, X. G.; Qi, L. M. Morphology-Controlled Synthesis of SnO_2 Nanotubes by Using 1D Silica Mesostructures as Sacrificial Templates and Their Applications in Lithium Ion Batteries. *Small* **2010**, *6*, 296–306.
24. Hu, Y. S.; Liu, X.; Müller, J. O.; Schlögl, R.; Maier, J.; Su, D. S. Synthesis and Electrode Performance of Nanostructured V_2O_5 by Using a Carbon Tube-in-Tube as a Nanoreactor and an Efficient Mixed-Conducting Network. *Angew. Chem., Int. Ed.* **2009**, *48*, 210–214.
25. Ng, S. H.; Wang, J. Z.; Wexler, D.; Konstantinov, K.; Guo, Z. P.; Liu, H. K. Highly Reversible Lithium Storage in Spheroidal Carbon-Coated Silicon Nanocomposites as Anodes for Lithium-Ion Batteries. *Angew. Chem., Int. Ed.* **2006**, *45*, 6896–6899.
26. Hu, Y. S.; Demir-Cakan, R.; Titirici, M. M.; Müller, J. O.; Schlögl, R.; Antonietti, M.; Maier, J. Superior Storage Performance of a Si@SiO_x/C Nanocomposite as Anode Material for Lithium-Ion Batteries. *Angew. Chem., Int. Ed.* **2008**, *47*, 1645–1649.
27. Deng, D.; Lee, J. Y. Reversible Storage of Lithium in a Rambutan-like Tin−Carbon Electrode. *Angew. Chem., Int. Ed.* **2009**, *48*, 1660–1663.
28. Cui, L. F.; Yang, Y.; Hsu, C. M.; Cui, Y. Carbon−Silicon Core−Shell Nanowires as High Capacity Electrode for Lithium Ion Batteries. *Nano Lett.* **2009**, *9*, 3370–3374.
29. Lee, H.; Kim, H.; Doo, S. G.; Cho, J. Synthesis and Optimization of Nanoparticle Ge Confined in a Carbon Matrix for Lithium Battery Anode Material. *J. Electrochem. Soc.* **2007**, *154*, A343–A346.
30. Gao, B.; Sinha, S; Fleming, L.; Zhou, O. Alloy Formation in Nanostructured Silicon. *Adv. Mater.* **2001**, *13*, 816–819.
31. Nam, K. T.; Kim, D. W.; Yoo, P. J.; Chiang, C. Y.; Meethong,

N.; Hammond, P. T.; Chiang, Y. M.; Belcher, A. M. Virus-Enabled Synthesis and Assembly of Nanowires for Lithium Ion Battery Electrodes. *Science* **2006**, *312*, 885–888.
32. Hamaoui, B. E.; Zhi, L. J.; Wu, J. S.; Kolb, U.; Müllen, K. Uniform Carbon and Carbon/ Cobalt Nanostructures by Solid-State Thermolysis of Polyphenylene Dendrimer/Cobalt Complexes. *Adv. Mater.* **2005**, *17*, 2957–2960.
33. Zhi, L. J.; Hu, Y. S.; Hamaoui, B. E.; Wang, X.; Lieberwirth, I.; Kolb, U.; Maier, J.; Müllen, K. Precursor-Controlled Formation of Novel Carbon/Metal and Carbon/Metal Oxide Nanocomposites. *Adv. Mater.* **2008**, *20*, 1727–1731.
34. Poizot, P.; Laruelle, S.; Grugeon, S.; Dupont, L.; Tarascon, J. M. Nano-Sized Transition-Metal Oxides as Negative-Electrode Materials for Lithium-Ion Batteries. *Nature* **2000**, *407*, 496–499.
35. Du, N.; Zhang, H.; Chen, B. D.; Wu, J. B.; Ma, X. Y.; Liu, Z. H.; Zhang, Y. Q.; Yang, D. R.; Huang, X. H.; Tu, J. P. Porous Co_3O_4 Nanotubes Derived From $Co_4(CO)_{12}$ Clusters on Carbon Nanotube Templates: A Highly Efficient Material For Li-Battery Applications. *Adv. Mater.* **2007**, *19*, 4505–4509.
36. Jiao, F.; Shaju, K. M.; Bruce, P. G. Synthesis of Nanowire and Mesoporous Low-Temperature $LiCoO_2$ by a Post-Templating Reaction. *Angew. Chem., Int. Ed.* **2005**, *44*, 6550–6553.
37. Li, W. Y.; Xu, L. N.; Chen, J. Co_3O_4 Nanomaterials in Lithium-Ion Batteries and Gas Sensors. *Adv. Funct. Mater.* **2005**, *15*, 851–857.